Diffuse Hard X-ray Sources Discovered with the *ASCA* Galactic Plane Survey

Aya Bamba, Masaru Ueno, and Katsuji Koyama,

Department of Physics, Graduate School of Science, Kyoto University, Sakyo-ku, Kyoto 606-8502, Japan

`bamba@cr.scphys.kyoto-u.ac.jp`, `masaru@cr.scphys.kyoto-u.ac.jp`, `koyama@cr.scphys.kyoto-u.ac.jp`

and

Shigeo Yamauchi

Faculty of Humanities and Social Sciences, Iwate University, 3-18-34 Ueda, Morioka, Iwate 020-8550, Japan

`yamauchi@iwate-u.ac.jp`

ABSTRACT

We found diffuse hard X-ray sources, G11.0+0.0, G25.5+0.0, and G26.6−0.1 in the *ASCA* Galactic plane survey data. The X-ray spectra are featureless with no emission line, and are fitted with both models of a thin thermal plasma in non-equilibrium ionization and a power-law function. The source distances are estimated to be 1–8 kpc, using the best-fit $N_{\rm H}$ values on the assumption that the mean density in the line of sight is 1 H cm^{-3}. The source sizes and luminosities are then 4.5–27 pc and $(0.8\text{–}23)\times10^{33}$ ergs s^{-1}. Although the source sizes are typical to supernova remnants (SNR) with young to intermediate ages, the X-ray luminosity, plasma temperature, and weak emission lines in the spectra are all unusual. This suggests that these objects are either shell-like SNRs dominated by X-ray synchrotron emission, like SN 1006, or, alternatively, plerionic SNRs. The total number of these classes of SNRs in our Galaxy is also estimated.

Subject headings: acceleration of particles — supernova remnants: individual (G11.0+0.0, G25.5+0.0, G26.6−0.1) — X-rays: ISM

1. Introduction

Since the discovery of cosmic rays (Hess 1912), the origin and the acceleration mechanism up to TeV or even more have been long-standing problems. The plausible acceleration sites in our Galaxy are shell-type SNRs with diffusive shock acceleration mechanism (Wentzel 1974; Reynolds et al. 1998), pulsars and pulsar wind nebulae (de Jager & Harding 1992), although Reynolds & Keohane (1999) suggests that no SNR can accelerate electrons up to $10^{15.5}$ eV (the "knee" energy). Both of them are characterized by hard X-rays via synchrotron radiation and we have already several samples of such SNRs: SN 1006 and some other SNRs which accelerate cosmic rays on their shell (Koyama et al. 1995, 1997; Slane et al. 1999; Bamba et al. 2000; Borkowski et al. 2001b; Slane et al. 2001) and the plerionic SNRs (Asaoka & Koyama 1990; Weisskopf et al. 2000; Blanton & Helfand 1996). Together with the discoveries of inverse Compton γ-rays, which are up-scattered cosmic microwave photons or synchrotron X-rays by the high energy electrons (Tanimori et al. 1998; Muraishi et al. 2000; Enomoto et al. 2002; Weekes et al. 1989), the hard X-ray emission supports the presence of extremely high energy electrons. The total and maximum energy of accelerated electrons in SN 1006 has been studied by *ASCA* (Allen, Petre, & Gotthelf 2001; Dyer et al. 2001) and *Chandra* (Bamba et al. 2003). In order to account for the total flux of the Galactic high energy cosmic rays, a large numbers of SNRs with non-thermal X-rays must be still hidden in the Galactic plane and should be discovered.

The maximum electron energy in the SNRs is determined by the balance between the acceleration and radiative energy loss. The acceleration rate is proportional to the magnetic field strength (B). However, the synchrotron energy loss is proportional to B^2 and electron energy. Ages of SNRs, densities of circumstellar matter, and explosion energies also limit the maximum energy. Since the synchrotron X-rays are produced by electrons with higher energy than those responsible to the radio emission, SN 1006-like SNRs should have relatively weak magnetic field (B), and they must be generally radio faint SNRs like SN 1006. In fact, new SN 1006-like SNRs such as G347.3−0.5, G266.2−1.2, and G28.6−0.1 are first found with X-rays, then later identified as radio faint SNRs (Koyama et al. 1997; Slane et al. 1999; Bamba et al. 2001a; Koyama et al. 2001). For the plerionic SNRs, the relation between the luminosity in X-ray and radio band is an unknown problem (Hands et al. 2001). For example, 3C58 has the radio luminosity 1000 times smaller than the Crab Nebula although both are strong X-ray emitters (Green 2001). Accordingly, the previous search for SNRs based on the radio observations (Green 2001) may not be the most optimized method.

We thus have searched for diffuse hard X-ray sources in the Galactic plane survey with *ASCA* (Sugizaki 1999), and found a handful of SNR candidates with hard X-rays. We have carried out long exposure observations on the selected 4 candidates to investigate whether or not these are new SNRs. One of the candidates, AX J1843.8−0352, is already identified as a new SN 1006-like SNR (Bamba et al. 2001a) with the aid of the radio continuum emission of G28.6−0.1 (Helfand et al. 1989) and the result is confirmed by the *Chandra* follow-up observations (Koyama et al. 2001; Ueno et al. 2003).

This paper reports on the results on the other three candidates, (G11.0+0.0, G25.5+0.0, and G26.6−0.1) in § 3, and discusses the mechanisms of their X-ray emissions (see § 4.1 and § 4.2). The implications on the total number of SNRs with hard X-rays in our Galaxy are also discussed in § 4.3.

2. Observations and Data Reduction

The *ASCA* Galactic plane survey has covered the area of the Galactic plane of $|l| \leq 45\overset{\circ}{.}0$ and $|b| \leq 0\overset{\circ}{.}4$, with the exposure time of $\sim$ 10 ks each. In the mosaic map shown by Sugizaki (1999), we searched for SNRs in hard X-rays excluding about 10% of the surveyed area, which was suffered from stray lights of bright X-ray sources. We selected the 4 brightest diffuse hard X-ray sources and performed follow-up deep exposure observations. The observation dates and the on-axis positions are summarized in Table 1.

ASCA carried four XRTs (X-Ray Telescopes; Serlemitsos et al. 1995) with two GISs (Gas Imaging Spectrometers; Ohashi et al. 1996) and two SISs (Solid-state Imaging Spectrometers; Burke et al. 1994) on the focal planes. Since our targets are diffuse sources with sizes comparable to the SIS field of view (FOV), we do not refer to the SIS data in this paper. In all of the observations, GISs were operated in the nominal PH mode. We rejected the GIS data obtained in the South Atlantic Anomaly, in low cut-off rigidity regions ($<$ 6 GV), or when the target's elevation angle was low ($< 5^\circ$). Particle events were removed by the rise-time discrimination method (Ohashi et al. 1996). After these screenings, the total available exposure time of each observation is shown in Table 1. To increase the statistics, the data of the two detectors, GIS-2 and GIS-3, were co-added in the following study.

3. Analyses and Results

3.1. X-Ray Images and Source Detection

The GIS images in the 0.7–7.0 keV band around the SNR candidates are shown in Figure 1. Diffuse enhancements can be seen with the centers at about (l, b) = ($11\overset{\circ}{.}0$, $0\overset{\circ}{.}0$), ($25\overset{\circ}{.}5$, $0\overset{\circ}{.}0$), and ($26\overset{\circ}{.}6$, $-0\overset{\circ}{.}1$), hence are referred to as G11.0+0.0, G25.5+0.0, and G26.6−0.1.

Weak point-like sources No.1, 7, and 12 are detected in G11.0+0.0, G25.5+0.0, and G26.6−0.1, respectively. We also checked the *ROSAT*[1] and *Einstein*[2] point source catalogs and found only one source, 1RXS J184049.1−054336 in G26.6−0.1 (the same source as No.12) from 15 arcmin circles of the diffuse sources. The flux of these point-like sources contributes about 10% of the diffuse flux (see Appendix). We thus made the radial profiles in the 0.7–7.0 keV band including the point-like sources, then fitted with a Gaussian plus constant (for the background) model (Figure 2). The diffuse components are detected with the confidence level of 10.2σ for G11.0+0.0, 5.7σ for G25.5+0.0, and 7.5σ for G26.6−0.1, respectively. The best-fit FWHM is 12.2 (>6.3), 10.8 (>4.9), and 8.9 (>5.7) arcmin for G11.0+0.0, G25.5+0.0, and G26.6−0.1, respectively (parentheses indicate single-parameter 90% confidence regions). The FWHM sizes are significantly larger than that of the point spread function of *ASCA* GIS (3 arcmin), hence we confirm the diffuse nature for G11.0+0.0, G25.5+0.0, and G26.6−0.1.

To confirm the *ASCA* results, we checked the *ROSAT* all sky survey images[3]. However, no counterparts of G11.0+0.0 nor G25.5+0.0 is found, mainly because of the large absorption and/or short exposure time. As for G26.6−0.1, a *ROSAT* counterpart is found. However, no pointing observation was made. Thus all the available data with reasonable spatial resolution and exposure are provided solely from our *ASCA* observations, hence we concentrate on the *ASCA* results hearinafter.

3.2. X-ray Spectra

For the spectral analyses, we combined the survey and the follow-up observation data: obs.1 and 2 for G11.0+0.0, obs.3 and 4 for G25.5+0.0, and obs.5 and 6 for G26.6−0.1 (see Table 1). The spectra were made using the photons in the circular regions of diameters 15 arcmin for G11.0+0.0, and 12 arcmin for both G25.5+0.0 and G26.6−0.1, respectively, which are equal to $\sim 3\sigma$ width of the radial profiles (Figure 2). These source regions are shown with the solid circles in Figure 1. X-ray photons of point sources, No.1 for G11.0+0.0, No.7 for G25.5+0.0, and No.12 for G26.6−0.1, were extracted from a 3 arcmin radius circle each and were removed from the diffuse source data.

In order to properly subtract the Galactic ridge X-rays (Koyama et al. 1986; Kaneda

---

[1] Available at http://www.xray.mpe.mpg.de/cgi-bin/rosat/src-browser.

[2] Available at http://heasac.gsfc.nasa.gov/docs/einstein/archive/heao2_archive.html.

[3] Available at http://www.xray.mpe.mpg.de/cgi-bin/rosat/rosat-survey.

et al. 1997), the background data were extracted from the source free regions near to the targets with the same FOVs and at the same distance from the Galactic plane (dashed lines in Figure 1). For the background of G11.0+0.0, we selected the annual region between 9 and 12 arcmin radius, but excluded the circular regions of 6 arcmin radius around the sources No.3 and 4.

The background-subtracted spectra are shown in Figure 3. We see relatively flat spectra and no line feature. The spectra were fitted with two models of a thin thermal plasmas in non-equilibrium ionization (NEI) (Borkowski et al. 2001a), and a power-law function. The absorption column densities are calculated using the cross sections by Morrison & McCammon (1983) of solar abundances (Anders & Grevesse 1989). These two models are statistically acceptable for all the spectra. The best-fit parameters are given in Table 2, while the best-fit power-law models are shown in Figure 3 with the solid-line histograms.

3.3. Physical Parameters of the Diffuse Sources

We searched for radio, optical, and infrared (IR) counterparts from SIMBAD data base at the positions of the diffuse X-ray sources, G11.0+0.0, G25.5+0.0, and G26.6−0.1, but found no candidates. We therefore can not derive the source distances by the aid of the other wavelength information, and have to rely solely on our X-ray spectra. The absorption column densities of G11.0+0.0 and G26.6−0.1 are significantly smaller than, while that of G25.5+0.0 is comparable to that through the Galactic inner disk ($\sim 10^{23}$ H cm^{-2}; Ebisawa et al. 2001). Therefore, the former two sources are likely located at the near side of the Galactic plane, while the latter would be in the Galactic Scutum arm.

To be more quantitative, we assumed that the average density in our Galaxy toward the inner disk is 1 H cm^{-3} (Ebisawa et al. 2001) and estimated the distances using the best-fit absorption column densities in Table 2. The results together with the source diameters and total luminosities are listed in Table 3. Although the results are based on the best-fit power-law model, essentially no difference is found from those based on the NEI model.

4. Discussions

From the Table 3, we conclude that G11.0+0.0, G25.5+0.0, and G26.6−0.1 are diffuse Galactic sources with large sizes of 5–30 pc and moderate luminosities of 10^{33-34} erg s^{-1}. For the nature of these diffuse sources, a key question is whether the spectra are thermal or not. Unfortunately, the observed spectra can not constrain on this issue in the statistical point of view. We hence discuss both the cases in the following subsections.

4.1. Are Diffuse Sources Thermal ?

If the spectra are thermal, one possibility for the diffuse sources is unresolved emissions of many young stars in star forming regions. The typical example of this class, the Orion nebula, has the total X-ray luminosity of 10^{33} ergs s^{-1} and mean temperature of 3–4 keV (Yamauchi et al. 1996), which are in the error ranges of the diffuse sources (Table 2 and Table 3). Since G11.0+0.0 and G26.6−0.1 are in the near side of the Galactic ridge, they should be detected as emission nebulae or H II regions, but have no optical, IR, nor radio band counterparts. On the other hand, since G25.5+0.0 is at a far distance in the Galactic inner arm, no detection in the other wavelength may not be surprising. However the source size of $\sim$30 pc is exceptionally large as a star forming region. We thus conclude that the diffuse sources are not likely to be star forming regions.

Another possibility of the nature of G11.0+0.0, G25.5+0.0, and G26.6−0.1 are either shell-like SNRs in the adiabatic phase or mixed morphology SNRs of young to middle age (10^{2-3} years). Usual SNRs of this class emit thermal X-rays with the temperature < 1 keV. However, the spectra of G11.0+0.0 and G26.6−0.1 are very hard ($\sim$ several keV) and have no strong emission line from highly ionized ions, which are not in favor of thermal SNRs. On the other hand, G25.5+0.0 has relatively mild temperature and reasonable abundance.

Assuming a uniform density plasma sphere, we estimate the emission measures ($E.M.$), dynamical times (t=radius/sound velocity), electron densities (n_{e}), total masses (M), and thermal energies (E), which are listed in Table 4. We find that total masses of G11.0+0.0 and G26.6−0.1 are only a few solar, consistent with young SNRs of high temperature plasma. However the total energies are significantly smaller than the canonical supernova explosion. Therefore only small fraction of the explosion energy must be converted to the thermal energy, hence they may be in the earlier phase than adiabatic. In this case, the X-ray emitting plasma should be attributable to the SN ejecta with large metalicity, but the observations show no large metal excess. Thus thermal SNRs are unlikely for these diffuse sources.

For G25.5+0.0, the physical parameters are consistent with the adiabatic phase SNR, however the plasma density (< 0.1 H cm^{-3}) is too small as the interstellar gas in the Scutum Arm. We thus regard that a thermal SNR for this diffuse source is also unlikely.

4.2. Non-Thermal Diffuse Sources ?

We then discuss a possibility of non-thermal origin. The most likely case is SNRs with non-thermal X-rays, like SN 1006 and the Crab Nebula. In Table 3, we also list the physical parameters of a newly established SN 1006-like SNR, AX J1843.8$-$0352 = G28.6$-$0.1 (Bamba et al. 2001a), for comparison.

First, we discuss the possibility that they are SN 1006-like SNRs. Photon indices of G11.0+0.0 and G25.5+0.0 are ~ 2, which are smaller than those of typical SN 1006-like SNRs, SN 1006 itself, G347.3$-$0.5, and G266.6$-$1.2, but are similar to that of G28.6$-$0.1. This may indicate that the synchrotron X-rays are due to the electrons with higher energy than that of the acceleration cut-off, which is expected from the first-order Fermi acceleration (expected $\Gamma = 1.5$; Wentzel 1974). The diameters and total luminosities also resemble those of G28.6$-$0.1. These facts strongly support that at least G11.0+0.0 and G25.5+0.0 are SN 1006-like SNRs.

To establish the SN 1006-like SNRs, the presence of synchrotron radio emission is essential. However no cataloged radio source is found in the NRAO VLA Sky Survey 20 cm survey archival data[4]. If the magnetic field is weaker than the other SN 1006-like SNRs, the radio surface brightness would be below the current detection limit.

In order to estimate the radio flux band for the SN 1006-like SNRs, we tried the spectral fittings with a *srcut* model (Reynolds et al. 1998; Reynolds & Keohane 1999). The spectral index at 1 GHz was frozen to $\alpha = -0.5$, expected value by first-order Fermi acceleration. The fittings were statistically accepted and the best-fit parameters are listed in Table 2. We also tried the same fittings with $\alpha = -0.6$ and found no essential difference in the best-fit parameters. The best-fit flux density for each source suggests that the expected surface brightness at 1 GHz is 9.8×10^{-24}, 1.7×10^{-23}, and 9.8×10^{-24} W m^{-2}Hz^{-1}sr^{-1} for G11.0+0.0, G25.5+0.0, and G26.6$-$0.1, respectively. On the other hand, the minimum surface brightness of the cataloged radio SNRs in our survey field is 2×10^{-21} W m^{-2}Hz^{-1}sr^{-1} (for G3.8+0.3; Case & Bhattacharya 1998), which is similar to SN 1006 (3×10^{-21} W m^{-2}Hz^{-1}sr^{-1}; Long, Blair, & van den Bergh 1988; Winkler & Long 1997) and G347.3$-$0.5 (4×10^{-21}W m^{-2}Hz^{-1}sr^{-1}; Ellison, Slane, & Gaensler 2001; assuming $\alpha = -0.5$), but is two or three orders of magnitude larger than our new sources. Even the minimum surface brightness of the all cataloged radio SNRs is larger than our sample, 6.2×10^{-23} W m^{-2}Hz^{-1}sr^{-1} (for G156.2+5.7; Case & Bhattacharya 1998). Therefore, no radio counterpart for our new X-ray sources would be simple due to limited detection threshold of the current radio observations.

---

[4] Available at http://www.cv.nrao.edu/.

The power-law spectra and the luminosities (10^{34}–10^{35} ergs s^{-1}) suggest that the new sources are also Crab-like (plerionic) SNRs, although no radio pulsar is found (Chevalier 2000). The luminosity ratio between the radio and X-ray band is largely different among the plerionic SNRs: the radio luminosity of 3C58, for example is about 10 times smaller, while that of X-ray is about 1000 times smaller than that of the Crab Nebula (Hands et al. 2001). We estimated the expected surface brightness using the flux density of 3C58 and the Crab Nebula (Green 2001). For the 3C58-like case, the surface brightness of G11.0+0.0, G25.5+0.0, and G26.6−0.1 at 1 GHz is expected to be 2.5×10^{-20}, 5.1×10^{-20}, and 1.9×10^{-20} W $\mathrm{m}^{-2}\mathrm{Hz}^{-1}\mathrm{sr}^{-1}$, respectively. Since these values are larger than the detection limit in the surveyed region (see previous paragraph), we exclude the 3C58-like case. On the other hand, for the Crab-like case, their respective surface brightness becomes to be 7.3×10^{-23}, 1.5×10^{-22}, and 5.6×10^{-23} W $\mathrm{m}^{-2}\mathrm{Hz}^{-1}\mathrm{sr}^{-1}$. Therefore, a possibility of the Crab-like case can not be excluded.

The photon index of G26.6−0.1 is unreasonably small as a usual SNR. The diameter and the total luminosity are also smaller than those of G28.6−0.1 and the other SNR candidates with non-thermal X-rays. Thus G26.6−0.1 may be of different class. Similar nature to G26.6−0.1 is found with hard X-ray clumps (Uchiyama et al. 2002) of γ Cygni, an SNR interacting with molecular clouds (Fukui & Tatematsu 1988) and an EGRET source (Esposito et al. 1996); all the sizes ($\sim$ a few pc), photon indices (~ 1.2), and luminosities ($\sim 4\times10^{32}$ ergs s^{-1} in the 2.0–10.0 keV band) of the clumps resemble those of G26.6−0.1. Uchiyama et al. (2002) concluded the mechanism to be bremsstrahlung from MeV electrons colliding with dense clouds. This mechanism is usually accompanied by line emission, but no evidence for emission line from G26.6−0.1 is found. Assuming a wide band spectrum of G26.6−0.1 to be the same as γ-Cygni, we estimate the 0.1–2 GeV band flux to be 6.1×10^{-8} photons $\mathrm{cm}^{-2}\mathrm{s}^{-1}$. This value is smaller than the EGRET detection limit in our survey regions (Esposito et al. 1996). Therefore, no counterpart of a MeV source in the EGRET third catalog (Hartman et al. 1999) near at G26.6−0.1 gives no constraint on the above discussion. Thus to establish the non-thermal bremsstrahlung origin for G26.6−0.1, detection of molecular clouds and MeV-γ source near at G26.6−0.1 is essential.

4.3. How Many SNRs with Hard X-rays in Our Galaxy ?

We have found 4 diffuse X-ray sources, and their hard X-ray spectra are not consistent with SNRs dominated by thermal emission, but suggest either SN 1006-like, plerionic SNRs, or possibly SNRs dominated by non-thermal bremsstrahlung.

The *ASCA* Galactic plane survey covered the region of $|l| \leq 45^{\circ}\!.0$ and $|b| \leq 0^{\circ}\!.4$, but about 10% of the fields should be excluded for the faint source survey due to the stray lights from bright point sources. In the above survey region, we found 5 new SNRs; the 3 sources in this paper, G28.6−0.1 by Bamba et al. (2001a), and G347.3−0.5 by Koyama et al. (1997). Therefore the number of expected SNRs in the surveyed field is $5 \times \frac{1}{1-0.1} \sim 5.6$. If we assume that the spatial density of SNR is uniform in the inner Galactic disk of $|l| \leq 60^\circ\!\!.0$ and $|b| \leq 1^\circ\!\!.0$ field, then the expected number is $5.6 \times \frac{120}{90} \times \frac{2}{0.8} = 19$. Since the X-ray surface brightness of the new SNR is only 2–3 times of the background Galactic ridge emission, we may miss detections of more samples with lower surface brightness (see § 4.2). Thus the number of SNRs with non-thermal X-rays in our Galaxy would fur exceed 20.

We thank the anonymous referee for helpful comments. The authors are grateful to the *ASCA* Galactic plane survey team. Our particular thanks are due to K. Torii, J. Yokogawa, and K. Ebisawa for their fruitful discussions and comments. This search made use of the SIMBAD database operated by CDS at Strasbourg, France. A.B. and M.U. are supported by JSPS Research Fellowship for Young Scientists.

A. Serendipitous Sources

Thirteen point-like sources above the 6σ threshold are found in the same GIS fields as shown with crosses in Figure 1. Some have been already reported by Sugizaki et al. (2001), while the others are newly reported sources.

We performed the spectral analyses of the point-like sources. The source regions were selected as 3 arcmin circles except for sources No.1 and No.8. For these two sources, we made the source regions with the 1.5 arcmin circular regions around the sources, because the contaminations from G11.0+0.0 are large. We made background spectra from source free regions near the sources. We fitted the background-subtracted spectra with a power-law function and the results are summarized in Table 5.

REFERENCES

Allen, G.E., Petre, R., & Gotthelf, E.V. 2001, ApJ, 558, 739

Anders, E., & Grevesse, N. 1989, Geochim. Cosmochim. Acta, 53, 197

Asaoka, I., & Koyama, K. 1990, PASJ, 42, 625

Bamba, A., & Koyama, K. 1999, IAU Circ., 7324

Bamba, A., Tomida, H., & Koyama, K. 2000, PASJ, 52, 1157

Bamba, A., Ueno, M., Koyama, K., & Yamauchi, S. 2001a, PASJ, 53, L21

Bamba, A., Yokogawa, J., Ueno, M., Koyama, K., & Yamauchi, S. 2001b, PASJ, 53, 1179

Bamba, A., Yamazaki, R., Ueno, M., & Koyama, K. 2003, ApJ, submitted

Blanton, E.L., & Helfand, D.J. ApJ, 470, 961

Borkowski, K.J., Lyerly, W.J., & Reynolds, S.P. 2001a, ApJ, 548, 820

Borkowski, K.J., Rho, J., Reynolds, S.P., & Dyer, K.K. 2001b, ApJ, 550, 334

Burke, B.E., Mountain, R.W., Daniels, P.J., Dolat, V.S., & Cooper, M.J. 1994, IEEE Trans. Nucl. Sci., 41, 375

Case, G.L., & Bhattacharya, D. 1998, ApJ, 504, 761

de Jager, O.C., & Harding, A. K. 1992, ApJ, 396, 161

Chevalier, R.A. 2000, ApJ, 539, 45

Dowens, A. 1984, MNRAS, 210, 845

Dyer, K.K., Reynolds, S.P., Borkowski, K.J., Allen, G.E., & Petre, R. 2001, ApJ, 551, 439

Ebisawa, K., Maeda, Y., Kaneda, H., & Yamauchi, S. 2001, Science, 293, 1633

Ellison, D.C., Slane, P., Gaensler, B.M. 2001, ApJ, 563, 191

Enomoto, R., et al. 2002, Nature, 416, 823

Esposito, J.A., Hunter, S.D., Kanbachm G., & Sreekumar, P. 1996, ApJ, 461, 820

Fukui, Y. & Tatematsu, K. 1988, in SNRISM, 261

Green, D.A. 2001, A Catalogue of Galactic Supernova Remnants (2001 December version), (Cambridge, UK, Mullard Radio Astronomy Observatory) available on the WWW at http://www.mrao.cam.ac.uk/surveys/snrs/

Hands, A., Warwick, R., Watson, M., & Helfand, D. 2001, in the proceedings of "New Visions of the X-ray Universe in the XMM-Newton and Chandra Era", astroph/0202180

Hartman, R.C., Bertsch, D.L., Bloom, S.D., Chen, A.W., Deines-Jones, P., Esposito, J.A., Fichtel, C.E., Friedlander, D.P. et al. 1999, ApJS, 123, 79

Helfand, D.J., Velusamy, T., Becker, R.H., & Lockman, F.J. 1989, ApJ, 341, 151

Hertz, P., & Grindlay, J.P. 1988, AJ, 96, 233

Hess V.F. 1912, Phys. Zeits 13, 1084

Kaneda, H., Makishima, K., Yamauchi, S., Koyama, K., Matsuzaki, K., & Yamasaki, N.Y. 1997, ApJ, 491, 638

Koyama, K., Makishima, K., Tanaka, Y., & Tsunemi, H. 1986, PASJ, 38, 121

Koyama, K., Kinugasa, K., Matsuzaki, K., Nishiuchi, M., Sugizaki, M., Torii, K., Yamauchi, S., & Aschenbach, B. 1997, PASJ, 49, L7

Koyama, K., Petre, R., Gotthelf, E.V., Hwang, U., Matsura, M., Ozaki, M., & Holt S.S. 1995, Nature, 378, 255

Koyama, K., Ueno, M., Bamba, A., Ebisawa, K. 2001, in the proceedings of "New Visions of the X-ray Universe in the XMM-Newton and Chandra era", ESTEC, Noordwijk, Netherlands, astroph/0202009

Long, K.S., Blair, W.P., & van den Bergh, S. 1988, ApJ, 333, 749

Morrison, R., & McCammon, D. 1983, ApJ, 270, 119

Muraishi, H., Tanimori, T., Yanagita, S., Yoshida, T., Moriya, M., Kifune, T., Dazeley, S.A., Edwards, P.G. et al. 2000, A&A, 354, L57

Ohashi, T., Ebisawa, K., Fukazawa, Y., Hiyoshi, K., Horii, M., Ikebe, Y., Ikeda, H., Inoue, H., et al. 1996, PASJ, 48, 157

Reynolds, S.P. 1998 ApJ, 493, 375

Reynolds, S.P., & Keohane, J.W. 1999, ApJ, 525, 368

Serlemitsos, P.J., Jalota, L., Soong, Y., Kunieda, H., Tawara, Y., Tsusaka, Y., Suzuki, H., Sakima, Y., et al. 1995, PASJ, 47, 105

Slane, P., Gaensler, B.M., Dame, T.M., Hughes, J.P., Plucinsky, P.P., & Green, A. 1999, ApJ, 525, 357

Slane, P., Hughes, J.P., Edgar, R.J., Plucinsky, P.P., Miyata, E., Tsunemi, H., Aschenbach, B. 2001, 548, 814

Sugizaki, M., 1999, Ph.D. Thesis, University of Tokyo

Sugizaki, M., Mitsuda, K., Kaneda, H., Matsuzaki, K., Yamauchi, S., & Koyama, K. 2001, ApJS, 134, 77

Tanimori, T., Hayami, Y., Kamei, S., Dazeley, S.A., Edwards, P.G., Gunji, S., Hara, S., Hara, T. et al. 1998, ApJ, 497, L25

Torii, K., Tsunemi, H., Dotani, T., & Mitsuda, K. 1997, ApJ, 489, L145

Uchiyama, Y. Takahashi, T., Aharonian, F., Mattox, J. 2002, ApJ, 571, 866

Ueno, M., Bamba, A., Koyama, K., & Ebisawa, K. 2003, ApJ, accepted (preprint doi:10.1086/368355), astroph/0301514

Voges, W., Aschenbach, B., Boller, T., Braeuninger, H., Briel, U., Burkert, W., Dennerl, K., Englhauser, J., et al. 1999, A&A, 349, 389

Weekes, T.C., et al. 1989, ApJ, 342, 379

Weisskopf, M.C., et al. 2000, ApJ, 536, L81

Wentzel, D.G. 1974, A&A Rev., 12, 71

Winkler, F.P., & Long, K.S. 1997, ApJ, 491, 829

Yamauchi, S., Koyama, K., Sakano, M., & Okada, K. 1996, PASJ, 48, 719

This preprint was prepared with the AAS LaTeX macros v5.0.

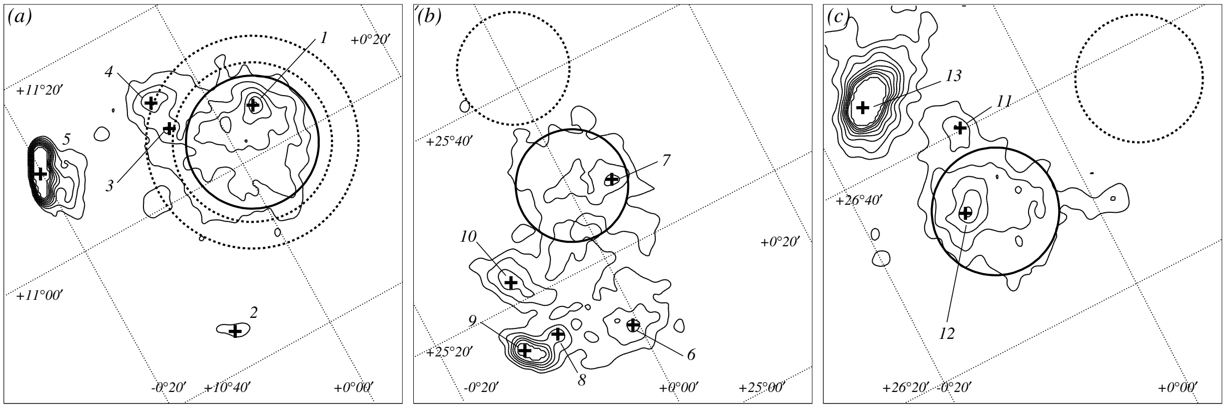

Fig. 1.— The GIS images with Galactic coordinates around G11.0+0.0 (a), G25.5+0.0 (b), and G26.6−0.1 (c) in the 0.7–7.0 keV band, where exposure time and vignetting effect are corrected. The images are smoothed with a Gaussian profiles of $\sigma = 0.5$ arcmin. The contour levels are linearly spaced with 6.4×10^{-4} counts arcmin^{-2} interval from the lowest level of 1.9×10^{-3} counts arcmin^{-2}s^{-1} for G11.0+0.0, 1.5×10^{-3} counts arcmin^{-2}s^{-1} for G25.5+0.0, and 2.4×10^{-3} counts arcmin^{-2}s^{-1} for G26.6−0.1. For bright point sources, the higher contour levels are truncated. The source and background regions for the spectral study (see text) are shown with the solid and dashed-line circles. The crosses indicate the position of point-like sources shown in Appendix (Table 5).

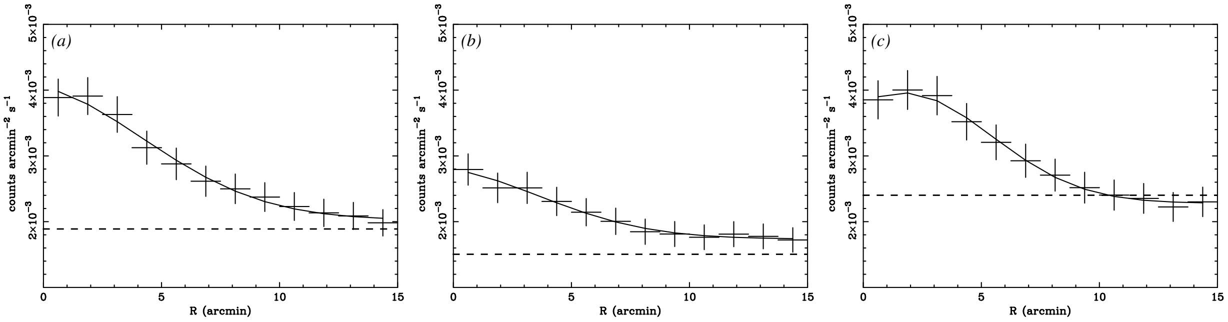

Fig. 2.— The radial profiles (crosses) of G11.0+0.0 (a), G25.5+0.0 (b), and G26.6−0.1 (c) after correcting the vignetting effect. Solid lines are the best-fit curves (see text). The dashed lines show the lowest contour level in Figure 1. The units of horizontal and vertical axes are arcmin from the center and counts arcmin^{-2} s^{-1}, respectively.

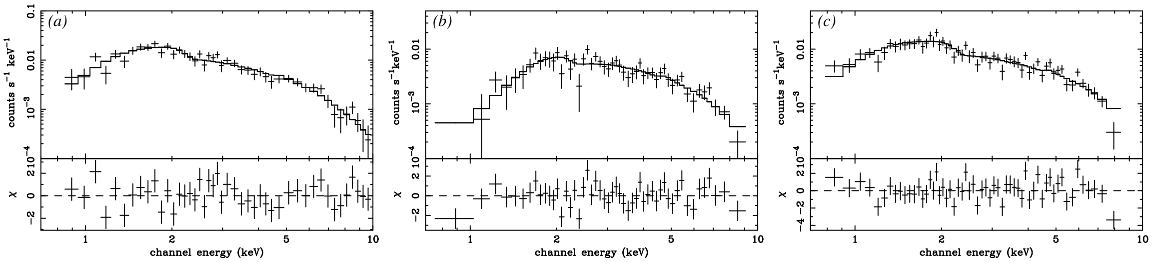

Fig. 3.— Upper panels: Background-subtracted spectra (crosses). (a: G11.0+0.0; b: G25.5+0.0; c: G26.6−0.1). The spectra of GIS 2 and 3 are combined. The solid lines are the best-fit power-law models. Lower panels: The data residuals from the best-fit models.

Table 1. Log of Galactic plane survey and follow-up deep observations.

Position (J2000) (RA, DEC)	Date (UT) yyyy/mm/dd	Exposure [ks]	Obs. Type	Obs. No.
$(18^{\rm h}09^{\rm m}50\overset{\rm s}{.}4, -19^{\circ}24'39\overset{''}{.}6)$	1996/08/04	10.3	survey	1
$(17^{\rm h}46^{\rm m}52\overset{\rm s}{.}8, -30^{\circ}02'31\overset{''}{.}2)$	1999/09/28	39.0	follow-up	2
$(18^{\rm h}37^{\rm m}48\overset{\rm s}{.}0, -06^{\circ}36'41\overset{''}{.}8)$	1997/10/14	12.4	survey	3
$(18^{\rm h}37^{\rm m}45\overset{\rm s}{.}6, -06^{\circ}36'43\overset{''}{.}2)$	1999/09/28	37.3	follow-up	4
$(18^{\rm h}39^{\rm m}43\overset{\rm s}{.}2, -05^{\circ}42'57\overset{''}{.}6)$	1997/04/20	9.8	survey	5
$(18^{\rm h}40^{\rm m}14\overset{\rm s}{.}4, -05^{\circ}40'44\overset{''}{.}4)$	1999/10/03	35.9	follow-up	6

Table 2. The best-fit parameters of the diffuse sources.[a]

	G11.0+0.0	G25.5+0.0	G26.6−0.1	G28.6−0.1[b]
Power-law Model				
Photon Index	1.6 (1.4–1.9)	1.8 (1.6–2.2)	1.3 (1.2–1.5)	2.1 (1.7–2.4)
Absorption Column Density [10^{22} H cm^{-2}]	0.8 (0.5–1.1)	2.4 (1.8–3.2)	0.4 (0.2–0.6)	2.7 (2.0–3.5)
Flux[c][ergs cm^{-2} s^{-1}]	3.8×10^{-12}	2.0×10^{-12}	3.5×10^{-12}	1.8×10^{-12}
χ^2/degrees of freedom	44.2/42	55.4/48	73.2/55	45.4/47
srcut Model[d]				
Break Frequency [$\times 10^{19}$Hz]	3.2 (> 0.4)	0.4 (0.07–36)	1.3×10^3 (> 12)	···
Flux Density[e][mJy]	9.0 (8.4–9.6)	9.6 (8.8–11)	5.6 (5.2–5.9)	···
Absorption Column Density [10^{22} H cm^{-2}]	0.8 (0.6–0.9)	2.3 (2.0–2.7)	0.6 (0.4–0.7)	···
χ^2/degrees of freedom	45.3/42	55.3/48	75.6/55	···
NEI Model				
Temperature [keV]	11.5 (7.3–21.0)	7.1 (4.5–14.0)	14.5 (8.7–34.8)	4.4 (3.3–6.2)
Abundance	0.7 (0.1–1.8)	0.4 (0.1–0.7)	0.5 (0.1–1.1)	1.7 (0.5–3.4)
$n_e t$ [10^9 s cm^{-3}]	0.9 (< 4.2)	3.2×10^2 (> 58)	5.1 (3.0–9.1)	1.1 (0.4–1.9)
Absorption Column Density [10^{22} H cm^{-2}]	0.6 (0.4–1.1)	2.3 (1.8–3.0)	0.9 (0.5–1.4)	3.9 (3.0–4.9)
Flux[c][ergs cm^{-2} s^{-1}]	3.8×10^{-12}	2.0×10^{-12}	3.4×10^{-12}	1.7×10^{-12}
χ^2/degrees of freedom	42.7/40	48.8/46	63.5/53	31.1/45

[a] Parentheses indicate single-parameter 90% confidence regions.

[b] Cited from Bamba et al. (2001a).

[c] In the 0.7–10.0 keV band.

[d] The radio spectral index is fixed to 0.5.

[e] At 1 GHz band.

Table 3. The physical parameters of the diffuse sources.

	G11.0+0.0	G25.5+0.0	G26.6−0.1	G28.6−0.1[a]
Distance[b][kpc]	2.6	7.8	1.3	7.0
Diameter [pc]	11	27	4.5	20
Luminosity[c][ergs s^{-1}]	3.7×10^{33}	2.3×10^{34}	8.1×10^{32}	2.2×10^{34}

[a] Cited from Bamba et al. (2001a).

[b] Calculated from the best-fit absorption column assuming that the mean density in the Galactic plane is 1 H cm^{-3}

[c] In the 0.7–10.0 keV band.

Table 4. The parameters for thermal plasma scenario.

Parameters	G11.0+0.0	G25.5+0.0	G26.6−0.1
Emission measure ($E.M.$)[a][cm^{-3}]	2.3×10^{56}	1.5×10^{57}	4.9×10^{55}
Dynamical time (t)[b][s]	1.3×10^{11}	3.9×10^{11}	4.7×10^{10}
Electron density (n_e) [cm^{-3}]	0.11	0.070	0.18
Total mass (M) [$M_\odot$]	1.8	18	2.3
Thermal energy (E)[c][ergs]	1.2×10^{50}	7.3×10^{50}	1.9×10^{49}

[a] $E.M. = n_\mathrm{e}^2 V$, where n_e is the electron density and V is the plasma volume.

[b] The ratio of the radius and the sound velocity.

[c] $E = \frac{3}{2}(n_\mathrm{i}+n_\mathrm{e})VkT$, where n_i is the ion density.

Table 5. The best-fit parameters of serendipitously detected sources.[a]

No.	Name	Photon Index	Absorption Column [10^{22} H cm^{-2}]	Flux[b] [ergs cm^{-2} s^{-1}]	Reduced χ^2
1 ...	AX J1809.7−1918	3.1(1.9–5.0)	1.6 (0.4–3.3)	3.1×10^{-13}	9.1/16
2 ...	AX J1809.8−1943	8.8 (>5.9)	1.7 (0.7–2.5)	6.1×10^{-13}	9.8/20
3 ...	AX J1810.4−1921	2.2 (1.5–3.2)	0.6 (0.1–1.4)	6.3×10^{-13}	15.4/17
4 ...	AX J1810.5−1917	3.4 (2.4–4.8)	0.5 (<1.3)	5.7×10^{-13}	11.7/17
5 ...	AX J1811.4−1926	...	...	...	...
6 ...	AX J1837.3−0652	2.3 (1.6–3.2)	5.9 (3.8–9.0)	1.8×10^{-12}	43.1/42
7 ...	AX J1837.4−0637	0.8 (0.5–1.1)	0.5 (0.1–1.2)	9.3×10^{-13}	48.8/59
8 ...	AX J1837.5−0653	1.1 (0.5–1.9)	5.3 (2.8–8.8)	4.1×10^{-12}	20.6/29
9 ...	AX J1838.0−0655	0.8 (0.4–1.2)	4.0 (2.8–5.7)	1.1×10^{-11}	12.9/12
10 ..	AX J1838.1−0648	2.1 (1.6–2.8)	3.9 (2.7–5.6)	1.5×10^{-12}	48.3/47
11 ..	AX J1840.4−0537	3.4 (>1.6)	0.6 (<4.0)	1.4×10^{-13}	6.8/13
12 ..	AX J1840.4−0545	2.3 (0.9–4.7)	5.8 (1.7–17.9)	6.2×10^{-13}	6.6/13
13 ..	AX J1841.0−0536	1.0 (0.3–1.9)	3.2 (1.1–6.4)	2.1×10^{-11}	13.2/21
13 ..	flare (obs.6)	1.1 (0.9–1.4)	7.2 (6.0–8.6)	9.5×10^{-11}	43.2/50

[a] Parentheses indicate single-parameter 90% confidence regions.

[b] In the 0.7–10.0 keV band.

Note. — No.1: Sugizaki et al. (2001) identified this source to an A type star HD166077, although the X-ray spectrum was much harder than those of normal stars. In this paper, we selected the background region around the source to remove the hard X-ray contamination from G11.0+0.0 and obtained a softer spectrum, consistent with a normal star.

No.2: The count rates and photon indices with *ROSAT* (Voges et al. 1999, 1RXS J189951.5194345) and *ASCA* (Sugizaki et al. 2001) are consistent with the present results.

No.4: AX J1810.5−1917 was brighter than AX J1810.4−1921 in obs.1, but was fainter in obs.2 (see Table 1), hence is a transient or a variable source.

No.5: This source is a bright SNR both in the radio and X-ray bands (Dowens 1984) with a pulsar at the center (Torii et al. 1997). No pulsation is found with the FFT and epoch-folding search, which may be due to the limited statistics. Also no spectral analyses is available due to location at the edge of the GIS FOV.

No.9: This is the *Einstein*, IPC (Hertz & Grindlay 1988) and *ASCA* (Sugizaki et al. 2001) source. The count rates in all the observations have been constant.

No.13: This is a transient X-ray pulsar detected in both obs.5 (quiescent) and 6 (quiescent+flare). The 4.7 s-pulsation is found at the flare phase (Bamba & Koyama 1999; Bamba et al. 2001b).